Supplementary Information (SI) for Soft Matter.

Supporting Information: The fluid dynamics of a viscoelastic fluid dripping onto a substrate

Konstantinos Zinelis,[†,‡] Thomas Abadie,[¶] Gareth H. McKinley,[‡] and Omar K. Matar[*,†]

†*Department of Chemical Engineering, Imperial College London, London SW7 2AZ, United Kingdom.*

‡*Department of Mechanical Engineering, Massachusetts Institute of Technology, Cambridge, MA 02139, USA.*

¶*School of Chemical Engineering, University of Birmingham, Birmingham B15 2TT, United Kingdom.*

E-mail: o.matar@imperial.ac.uk

Summary

In the supporting materials, we provide important details on the grid cell resolution of the numerical simulations of a Dripping-onto-Substrate (DoS) experiment [1–3] and the fitting methods implemented for the determination of the relaxation time of a polymer using DoS rheometry. In the first section, we present the mesh convergence study for evaluating the accuracy of the numerical simulations using the code *Basilisk* [4] to describe the thinning dynamics of a viscoelastic filament in a DoS experiment. In the second section, we provide a qualitative comparison between the predictions of the "Anna-McKinley" empirical model [5] and the FENE-P analytical solution [6] in order to determine the apparent relaxation time of a dilute polymer solution and we also capture the effect of the Bond number, the macroscopic contact angle and the Deborah number on the fitting results. In the last section, we focus on the predictions of the FENE-P analytical solution and we carefully inspect the fitting results for the elastic modulus and the polymer chain extensibility.

Mesh Convergence Study

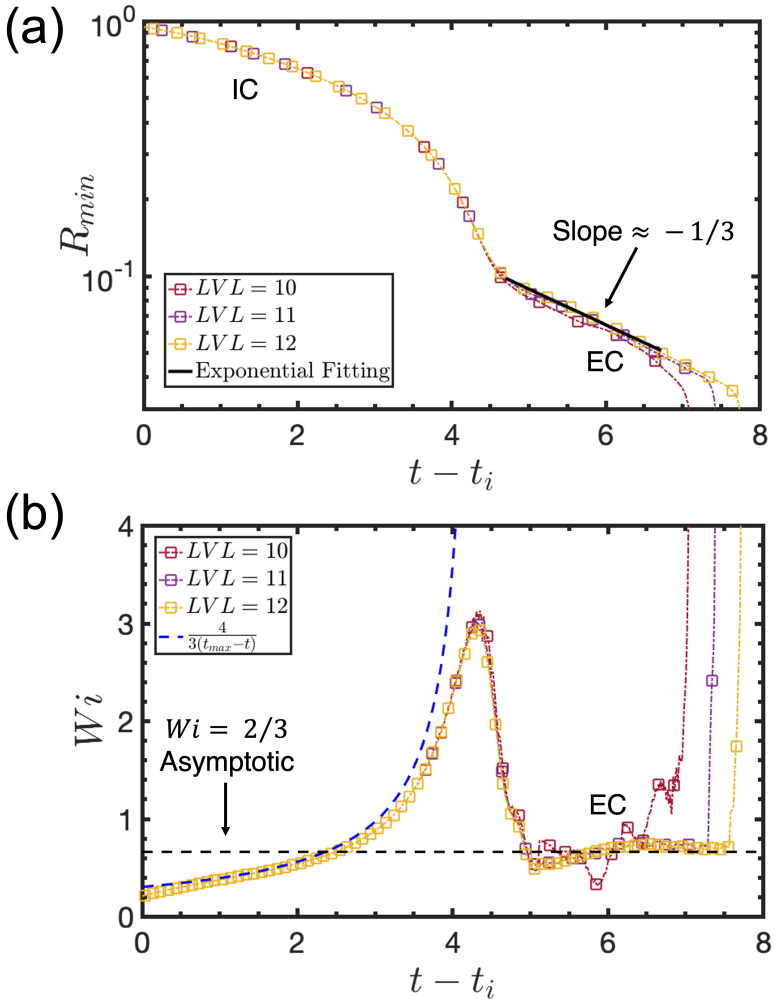

Figure S1: Mesh convergence study using three levels-of-refinement $LVL = 10$, 11 and 12 ($\Delta r_{minimum} = 0.0051$, 0.0026, and 0.0013) for the parameters shown in Table 1 (main text) for the numerical simulations of a thinning filament during a Dripping-onto-Substrate (DoS) experiment; results are presented through the temporal evolution of (a) the minimum filament radius $R_{min}(t)$, and (b) the evolution in the dimensionless strain rate $Wi(t) = \dot{\epsilon}(t)\tau$, in order to evaluate the resolution of the Inertio-Capillary (IC), the subsequent Elasto-Capillary (EC), and finally the Terminal Visco-Elasto-Capillary (TVEC) regimes. The Oldroyd-B asymptotic thinning rate[7–10](−1/3 slope) during the exponential thinning of the filament (black solid line), and the theoretical predictions for the filament dynamics during the IC regime (blue dashed line) are also shown in (a) and (b), respectively. Here, the dimensionless time scale t has been shifted by an initial offset, t_i which corresponds to the time at which the residual effects of the initial spreading process become negligible. The time when the local Wi attains its maximum value is denoted by $t_{max} - t_i = 4.29$ (with $t_{max} = 11.75$ and $t_i = 7.46$); this also coincides with the end of the IC regime and the subsequent transition to the EC regime.

We present in Figure S1 the capability of *Basilisk*[4] to resolve the filament thinning dynamics during a Dripping-onto-Substrate rheometry adequately, accounting for the wetting process of the substrate. Specifically, we show in Figure S1(a) and (b) the temporal profiles of the dimensionless minimum radius of the viscoelastic filament $R_{min}(t)$ and the local dimensionless strain rate $Wi(t) = \dot{\epsilon}(t)\tau$ respectively, with $\dot{\epsilon}(t) = -2d\log(R_{min})/dt$ and τ denotes the relaxation time of the polymer, for the same physical properties listed in Table 1 (main text) and for three different levels of refinement ($LVL = 10$, 11, and 12) which correspond to three distinct minimum square cell sizes ($\Delta r_{minimum} = 0.0051$, 0.0026, and 0.0013). In addition, in the current work, we treat the lateral spreading of the fluid over the solid substrate by setting the macroscopic equilibrium contact angle as a boundary condition on the solid boundary in combination with the height-function method[11]. Although we enforce a no-slip condition on the substrate, the velocity field for the interface advection is located at the centre of the cell faces and therefore *Basilisk*[4] allows for an implicit slip condition at the contact line singularity with slip length of $\Delta r_{minimum}/2$[11,12]. Hence, these three values of the refinement level (or the minimum cell sizes) also determine the resulting slip lengths at the contact line that can be resolved here (which at $LVL = 12$ are up to 4 orders of magnitude lower than the initial filament radius R_0).

In Figure S1 we observe that even though the profiles of $R_{min}(t)$ and $Wi(t)$ at $LVL = 10$ are seen to fluctuate more compared to $LVL = 11$ and 12, all the LVL values exhibit identical Inertio-Capillary (IC) dynamics, and converge to the Oldroyd-B asymptotic of $-1/(3De)$[7–10] (or equivalently $Wi = 2/3$) during the Elasto-Capillary (EC) regime. Moreover, at the highest level of refinement $LVL = 12$ (i.e. the lowest $\Delta r_{minimum} = 0.0013$), we do not observe any substantial difference during the exponential EC thinning of the filament. Mesh resolution limitations only become apparent in the terminal linear visco-elasto-capillary (TVEC) thinning at $t - t_i \geq 7$[9,13,14], which is beyond the scope of the current work. Therefore, at $LVL = 11$ ($\Delta r_{minimum} = 0.0026$) we can sufficiently resolve both the initial inertio-capillary thinning and the subsequent onset and evolution of the EC regime, which are the main focus

of this work. Finally, we also see that the macroscopic filament dynamics remain essentially unaffected by the magnitude of the slip length ($\sim 10^{-3}R_0$ for $LVL = 11$ and $\sim 10^{-4}R_0$ for $LVL = 12$) at the contact line singularity.

Fitting results with the Anna-McKinley model and the FENE-P analytical solution

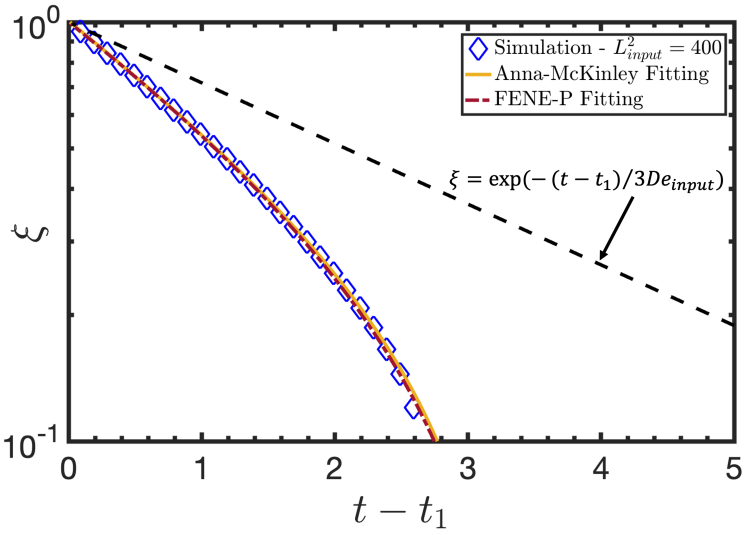

Figure S2: Simulation data of the dimensionless minimum filament radius ξ during the EC regime denoted by diamond symbols for a polymer finite extensibility $L^2_{input} = 400$, fixed Deborah number $De_{input} = \tau/t_R = 1$, and elasto-capillary number $Ec_{input} = \eta_p R_0/(\tau\gamma) = 0.03$. Here, the time t is shifted by t_1 which corresponds to the onset of the EC regime. The predictions of the Anna-McKinley fitting model (Eq. (18) in the main text) and the FENE-P analytical solution (Eq.(19) in the main text) for $L^2_{input} = 400$ are shown by solid orange and dashed red lines, respectively. The dashed black line corresponds to the prediction of exponential Oldroyd-B decay during the EC regime[9,15,16].

In Figure S2 we show the results obtained from fitting Eq. (18) labelled "Anna-Mckinley Fitting" (solid orange line) and Eq. (19) labelled "FENE-P Fitting" (dashed red line) to the data (blue diamonds) generated with the numerical simulations presented in this work for the evolution of the scaled filament radius $\xi = R_{min}(t)/R_1$ with time $t - t_1$, where R_1 and t_1 are the dimensionless filament radius and time at the onset of the EC regime, respectively.

The properties considered here are the same as in Table 1 (main text) but with the smallest finite extensibility of the polymer ($L^2 = 400$). We observe a significant deviation of the simulation and the predictions of the two fitting equations from the Oldroyd-B asymptotic result (dashed black line) during the EC regime. We also see that both Eq. (18) and (19) overlap very well with the simulation data qualitatively. However, Table 6 and Figure 12 (main text) reveal important quantitative differences that should be carefully considered when we aim to extract the apparent relaxation time of dilute polymer solutions with limited extensibility.

Here, we also examine the influence that the Bond number, the subsrtate wettability and the Deborah number can exert on the fitting results. We first show in Figure S3 the evolution of the dimensionless radius and the dimensionless strain rate in the viscoelastic filament for a finite Bond number ($Bo = 1$), a larger macroscopic contact angle ($\theta_E = 60°$) and a higher Deborah number ($De = 5$) than the main case presented in the main text while remaining at the smallest polymer finite extensibility ($L^2 = 400$). We also show a case for $De = 5$ but for the second smallest finite extensibility value ($L^2 = 900$). Hence, we focus on the finite chain extensibility values for which the largest deviations are seen, as presented thoroughly in Figure 4 and Table 6 in the main text. When we vary the Bond number or the macroscopic contact angle θ_E, we do not observe a strong effect on the resulting thinning-rate, while a larger polymer finite extensibility for the same Deborah number still deviates (but less so) from the Oldroyd-B asymptotic ($Wi = 2/3$). All these observations are consistent with the key results presented in the main text.

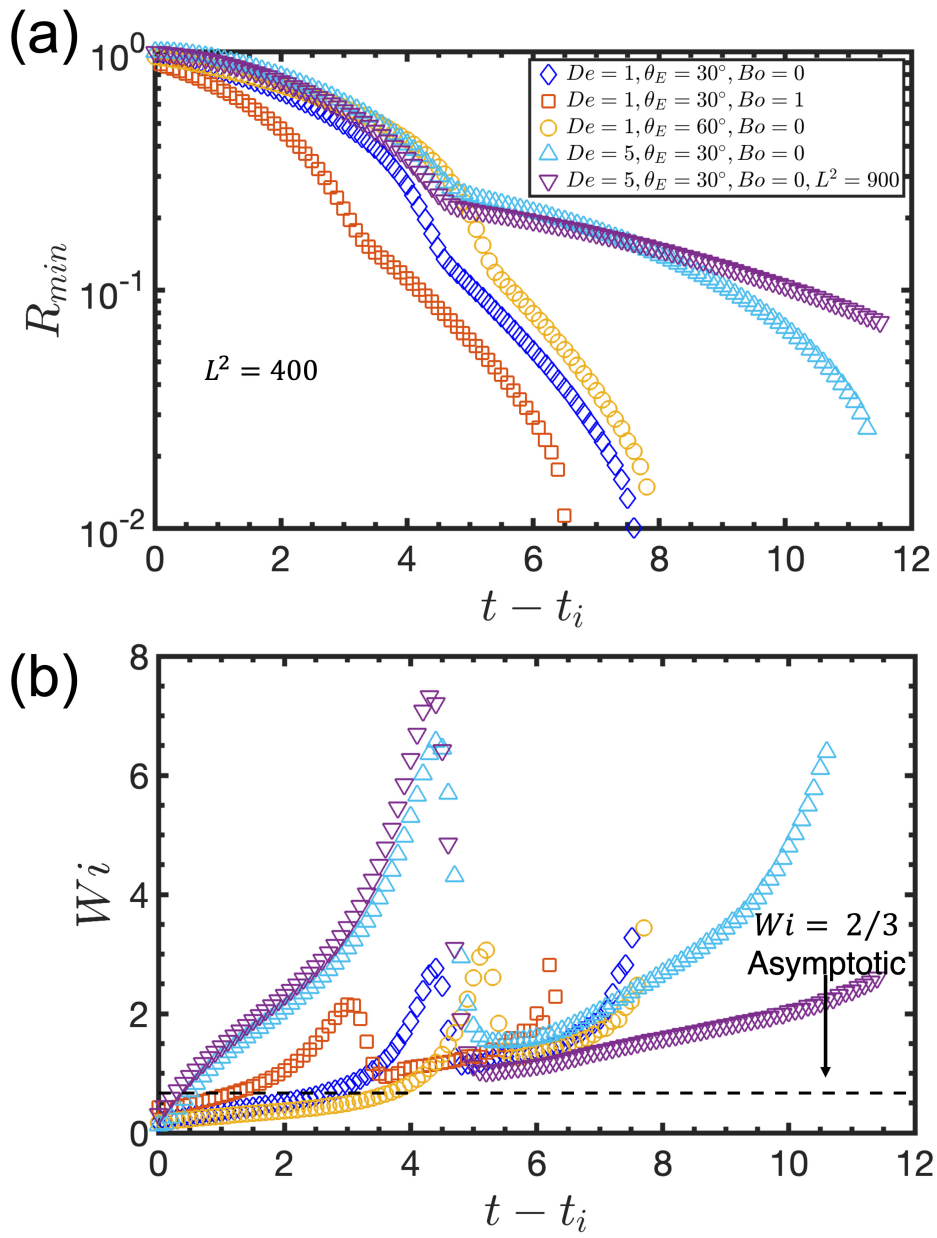

Figure S3: (a) Temporal profiles of the dimensionless minimum filament radius $R_{min}(t)$ and the local dimensionless strain rate $Wi(t) = \tau\dot{\epsilon}(t)$ for two Deborah numbers ($De = 1$ and 5), two Bond numbers ($Bo = 0$ and 1), two contact angles ($\theta_E = 30°$ and 60°), and polymer finite extensibility $L^2 = 400$ (and L^2=900 for $De = 5$ denoted by purple diamond symbols). The rest of the parameters remain unchanged from Table 1 in the main text.

Table S1: Determination of the dimensionless relaxation time of the polymer Deborah number (De) when we vary the Bond number, the substrate wettability and the Deborah number as inputs; Here, $(De_{input}, Ec_{input}, L^2_{input})$ are the known (ground truth) values that are used as inputs to the numerical simulations; $De_{fit}^{[Oldroyd-B]}$ and $De_{fit}^{[AM]}$ are the values of the dimensionless relaxation time obtained when we use the asymptotic Oldroyd-B result: $R_{min}(t) \sim \exp(-t/(3De)$ (labelled "Oldroyd-B Fitting") and the "Anna-McKinley" model provided in Eq. (18) in the main text (labelled "Anna-McKinley Fitting") to determine the dimensionless relaxation time of the dilute polymer solution from the data in the EC regime (here, we consider the data generated by the numerical simulations). $(De_{fit}^{[FENE]}, Ec_{fit}^{[FENE]}, L^{2[FENE]}_{fit})$ are the parameters obtained when Eq. (19) in the main text is fitted to the available data for the filament radius (labelled "FENE-P Fitting"). The errors $\epsilon^{[Oldroyd-B]}$, $\epsilon^{[AM]}$ and $\epsilon^{[FENE]}$ are the discrepancies in the prediction of the dimensionless polymeric relaxation time De_{fit} when either the Oldroyd-B result or Eq. (18)) or Eq. (19) in the main text, respectively are used.

Input					Oldroyd-B Fitting	Anna-McKinley Fitting	FENE-P Fitting	Error for De_{fit}		
De_{input}	Ec_{input}	L^2_{input}	Bo_{input}	θ_{Einput}	$De_{fit}^{[Oldroyd-B]}$	$De_{fit}^{[AM]}$	$De_{fit}^{[FENE]}$	$\epsilon^{[Oldroyd-B]}$	$\epsilon^{[AM]}$	$\epsilon^{[FENE]}$
1	0.03	400	0	30°	0.60	0.56 ± 0.02	0.70 ± 0.006	−40%	−44%	−30%
1	0.03	400	1	30°	0.66	0.51 ± 0.020	0.83 ± 0.030	−34%	−49%	−17%
1	0.03	400	0	60°	0.56	0.54 ± 0.030	0.66 ± 0.010	−44%	−46%	−34%
5	0.006	400	0	30°	2.20	3.93 ± 0.030	4.02 ± 0.030	−56%	−22%	−20%
5	0.006	900	0	30°	3.33	5.46 ± 0.020	5.13 ± 0.010	−33%	+9%	+3%

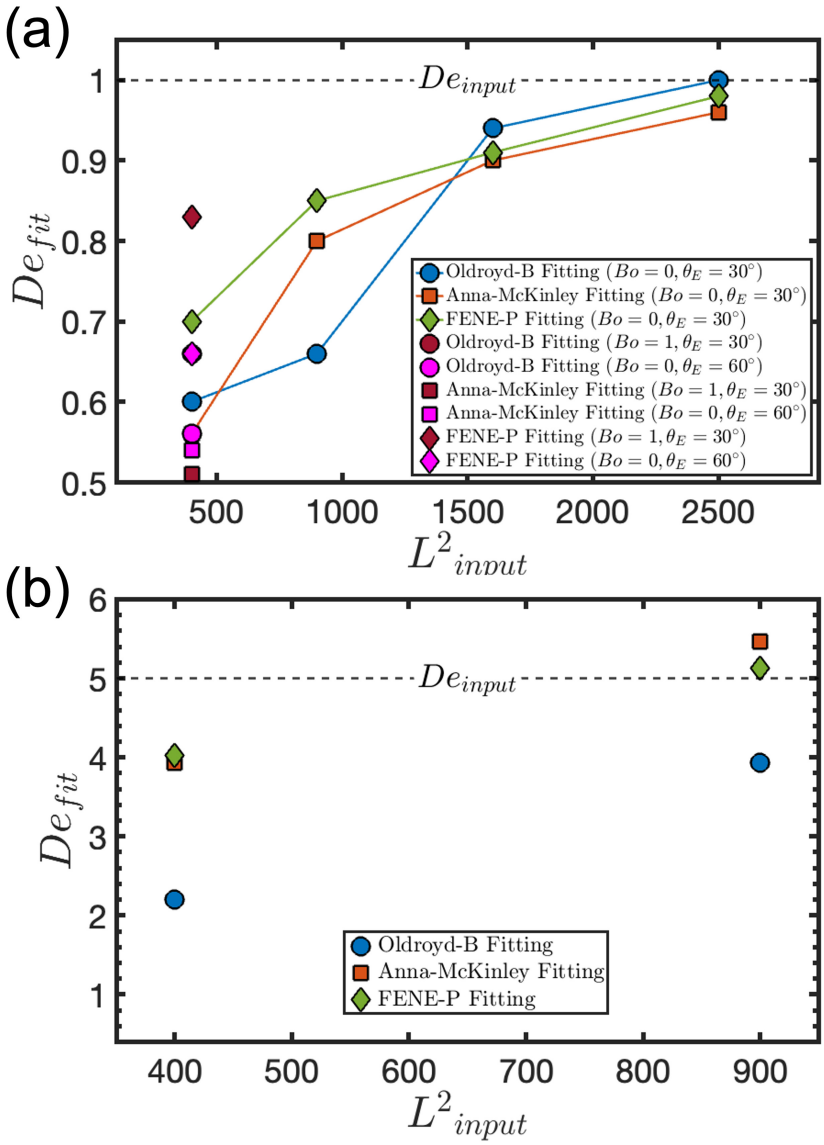

Figure S4: Estimated values of De_{fit} from Table S1 for (a) $L^2_{input} = \{400, 900, 1600, 2500\}$ and $De_{input} = 1$ (the results for a finite Bond number value and for a smaller substrate wettability are denoted by magenta and dark red colors, respectively), and (b) for $L^2 = 400$ and 900 and $De_{input} = 5$ using the "Oldroyd-B" (blue circles) , the "Anna-McKinley" (red squares) and the "FENE-P" (green diamonds) fitting approaches. The dashed black lines show the ground-truth values of $De_{input} = 1$ and $De_{input} = 5$, respectively.

In addition, we provide in Table S1 the fitting results employing the Oldroyd-B ($R_{min}(t) \sim \exp(-3t/De)$), Anna-McKinley (Eq. (18) in the main text) and FENE-P (Eq. (19) in the main text) fitting models for the cases shown in Figure S3. We also show in Figure S4 the predicted value of the dimensionless relaxation time of the polymer for the additional

cases and those presented already in the main text as it results from these methods. We observe that for the lowest finite extensibility of the polymer, the significant deviation from the input value De_{input} persists in all the cases independently of the magnitude of the Bond number, the substrate wettability and the Deborah number. We also see that the FENE-P fitting approach presents the smallest error compared with the Oldroyd-B prediction and the Anna-McKinley model, consistent with what is concluded in the main text.

More specifically, we observe that with a finite Bond number ($Bo = 1$) the Oldroyd-B and the FENE-P error decreases, while theerror incurred from using the Anna-McKinley model increases. Additionally, the fitting predictions slightly worsen for all the methods with a smaller substrate wettability (larger equilibrium contact angle). Finally, when we increase the Deborah number ($De = 5$), we see that at the smallest value of the polymer finite extensibility ($L^2 = 400$) the Anna-McKinley and the FENE-P analytical solution achieve similar levels of fidelity (while the Oldroyd-B is still the worst). However, the FENE-P fitting model seems more suitable when we move to a larger finite extensibility ($L^2 = 900$), as it incurs a fitting error of only around 3%. These observations allow us to conclude that with the use of the FENE-P analytical solution (Eq. (19) in the main text) we can improve (up to an extent) determination of the relaxation time of polymeric samples with very small finite extensibility values.

Analysis of the predictions of the FENE-P analytical solution

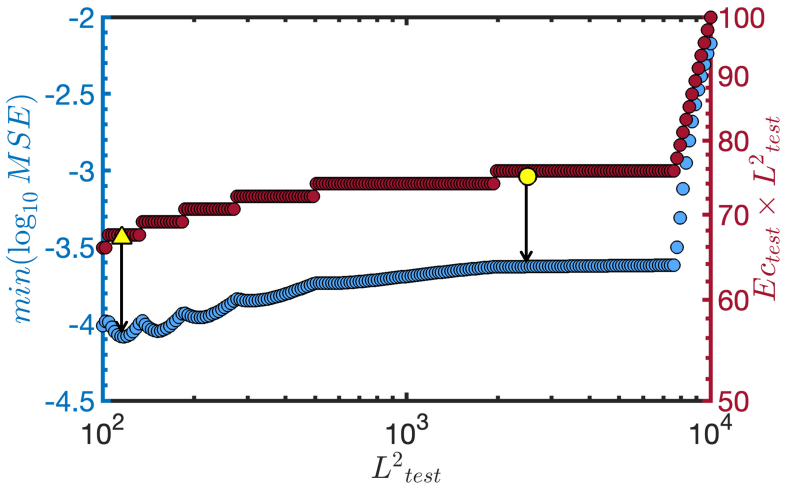

Figure S5: Minimum Mean Squared Error ($min(\log_{10} MSE)$) in blue and the combinations of the elasto-capillary number and polymer finite extensibility ($Ec_{test} \times L^2_{test}$). The values correspond to the minimum Mean Squared Error from the predictions of the FENE-P analytical solution for filament thinning during the EC regime for different values of polymer extensibility (L^2_{test}). The known input and the predicted values of the products ($Ec_{test} \times L^2_{test}$) are denoted by a yellow circle and triangle symbol, respectively. The black arrows point to the minimum Mean Squared Error, $min(\log_{10} MSE) \approx -3.7$ and $min(\log_{10} MSE) \approx -4$, of the known and predicted values ($Ec_{test} \times L^2_{test}$), respectively.

We present in Figure S5 the variation in the minimum Mean Squared Error (MSE), and the product ($Ec_{test} \times L^2_{test}$) of the different combinations of elasto-capillary numbers (which correspond to the dimensionless elastic modulus, $Ec = GR_0/\gamma$) and polymer extensibilities that result in the minimum MSE ($min(\log_{10} MSE)$). The error evolves continuously with the value of finite extensibilities L^2_{test} ($10^2 \leq L^2_{test} \leq 10^4$) considered in Figure 14 (main text). The product $Ec_{test} \times L^2_{test} = 75$ of the known (ground-truth) values ($Ec_{test} = 0.03, L^2_{test} = 2500$) is denoted by a yellow circle symbol in Figure S5, and results in a minimum MSE of $min(\log_{10} MSE) \approx -3.7$. These are the elasto-capillary number ($Ec_{test} = 0.03$) and finite extensibility value ($L^2_{test} = 2500$) that we expect from the predictions of Eq. (19) (main text). However, the optimiser of the fitting process using Eq. (19) detects a different value

of the minimum MSE. This value is $min(\log_{10} MSE) \approx -4$ and corresponds to the product $Ec_{test} \times L^2_{test} \approx 67.1$ ($Ec_{test} = 0.58, L^2_{test} = 115.7$) denoted by a yellow triangle symbol in Figure S5. Nonetheless, this systematic error in the prediction of the elasto-capillary number and polymer chain extensibility does not substantially affect the determination of the relaxation time of the polymer using the FENE-P analytical solution (Eq. (19) in the main text).

References

(1) Dinic, J.; Zhang, Y.; Jimenez, L. N.; Sharma, V. Extensional Relaxation Times of Dilute, Aqueous Polymer Solutions. *ACS Macro Lett.* **2015**, *4*, 804–808.

(2) Dinic, J.; Jimenez, L. N.; Sharma, V. Pinch-off dynamics and dripping-onto-substrate (DoS) rheometry of complex fluids. *Lab Chip* **2017**, *17*, 460–473.

(3) Dinic, J.; Sharma, V. Macromolecular relaxation, strain, and extensibility determine elastocapillary thinning and extensional viscosity of polymer solutions. *Proceedings of the National Academy of Sciences* **2019**, *116*, 8766–8774.

(4) Popinet, S. An accurate adaptive solver for surface-tension-driven interfacial flows. *J. Comput. Phys.* **2009**, *228*, 5838–5866.

(5) Anna, S. L.; McKinley, G. H. Elasto-capillary thinning and breakup of model elastic liquids. *Journal of Rheology* **2001**, *45*, 115–138.

(6) Wagner, C. E.; Bourouiba, L.; McKinley, G. H. An analytic solution for capillary thinning and breakup of FENE-P fluids. *J. Nonnewton. Fluid Mech.* **2015**, *218*, 53–61.

(7) Entov, V. M.; Yarin, A. L. Influence of elastic stresses on the capillary breakup of jets of dilute polymer solutions. *Fluid Dynamics* **1984**, *19*, 21—29.

(8) Bazilevesky, A.; Entov, V. M.; Rozhkov, A. N. Liquid filament microrheometer and some of its applications. *Proc. Third Eur. Rheol. Conf. (ed. D. R. Oliver)* **1990**, 41 Elsevier Applied Science.

(9) Entov, V. M.; Hinch, E. J. Effect of a spectrum of relaxation times on the capillary thinning of a filament of elastic liquid. *J. Nonnewton. Fluid Mech.* **1997**, *72*, 31–53.

(10) Tirtaatmadja, V.; McKinley, G. H.; Cooper-White, J. J. Drop formation and breakup of low viscosity elastic fluids: Effects of molecular weight and concentration. *Phys. Fluids* **2006**, *18*, 043101.

(11) Afkhami, S.; Bussmann, M. Height functions for applying contact angles to 3D VOF simulations. *Int. J. Numer. Methods Fluids* **2008**, 827–847.

(12) Snoeijer, J. H.; Andreotti, B. Moving Contact Lines: Scales, Regimes, and Dynamical Transitions. *Annual Review of Fluid Mechanics* **2013**, *45*, 269–292.

(13) McKinley, G. H. Visco-elasto-capillary thinning and break-up of complex fluids. *Rheol. Rev.* **2005**, *3*, 1–48.

(14) Wagner, C.; Amarouchene, Y.; Bonn, D.; Eggers, J. Droplet detachment and satellite bead formation in viscoelastic fluids. *Phys. Rev. Lett.* **2005**, *95*, 7–10.

(15) Clasen, C.; Eggers, J.; Fontelos, M. A.; Li, J.; McKinley, G. H. The beads-on-string structure of viscoelastic threads. *J. Fluid Mech.* **2006**, *556*, 283–308.

(16) Rajesh, S.; Thiévenaz, V.; Sauret, A. Transition to the viscoelastic regime in the thinning of polymer solutions. *Soft Matter* **2022**, *18*, 3147–3156.